

Dynamo-free plasma in the reversed field pinch

J. K. Anderson, T. M. Biewer, C. B. Forest, R. O'Connell, S. C. Prager, and J. S. Sarff

Department of Physics, University of Wisconsin-Madison, Madison, Wisconsin 53706

(Received 23 January 2004; accepted 13 February 2004; published online 13 April 2004)

Transient application of a poloidal electric field to reversed field pinch (RFP) plasmas has led to a period in which dynamo activity (inherent in standard RFP plasmas) nearly vanishes. Measurements of the plasma resistivity, current density and electric field profiles show the edge-applied electric field accommodates Ohm's law balance without a dynamo term over the entire cross section. Neoclassical theory accurately predicts the resistivity in the RFP, as the predicted resistivity profile (based on measurements of electron temperature, effective ionic charge, and two-dimensional equilibrium effects) is in agreement with the ratio of the parallel electric field and current density profiles. © 2004 American Institute of Physics. [DOI: 10.1063/1.1697399]

Conventional reversed field pinch (RFP) plasmas are formed via application of a toroidal electric field within a relatively weak toroidal magnetic field.¹ Internal redistribution of the current density leads to the well known equilibrium: a monotonically decreasing toroidal magnetic field profile which reverses direction at the extreme edge.^{2,3} The dynamo process—the self-generation of current—is thus inherent in the RFP;^{4–6} the applied electric field does not account for the current. This is most apparent outside the reversal layer where the applied electric field and current are antiparallel, as indicated in Fig. 1. In this standard RFP plasma, the magnetohydrodynamic (MHD) dynamo is responsible for driving the non-inductive current and the parallel Ohm's law $E_{\parallel} + \langle \tilde{\mathbf{v}} \times \tilde{\mathbf{b}} \rangle_{\parallel} = \eta J_{\parallel}$ is obeyed.⁷ Here, E_{\parallel} is the axisymmetric component of the applied electric field aligned with the magnetic field, J_{\parallel} is the field-aligned current density, and the nonlinear interaction of resistive MHD modes creates coherent magnetic field ($\tilde{\mathbf{b}}$) and velocity ($\tilde{\mathbf{v}}$) fluctuations which form a net parallel emf ($\langle \tilde{\mathbf{v}} \times \tilde{\mathbf{b}} \rangle_{\parallel}$).

Theoretical work⁸ has indicated that externally driven poloidal current in the RFP can stabilize the plasma to the tearing mode activity. Indeed, it has been previously reported that fluctuations have been reduced by inductively driving edge current.^{9,10} Magnetic fluctuation levels are reduced dramatically, thereby improving the electron energy confinement,¹¹ and measurements show a substantial drop in the $\langle \tilde{\mathbf{v}} \times \tilde{\mathbf{b}} \rangle_{\parallel}$ dynamo term in the plasma edge.¹²

In this paper, we report the production of a RFP plasma in which the dynamo is essentially absent, $E_{\parallel} = \eta J_{\parallel}$ over nearly the entire cross section. This result has implications on RFP performance: it is demonstrated that a fluctuation-driven dynamo (and the accompanying confinement degradation) is not required for existence of the high β RFP configuration. The dynamo-free periods occur during pulsed poloidal current drive (PPCD) experiments in the Madison Symmetric Torus (MST)¹³ RFP. The toroidal field windings are pulsed in a sense to remove toroidal flux from the machine and the inductive response of the plasma drives parallel (poloidal) current in the edge. The modification of the current profile stabilizes the plasma to the tearing modes, and

the need for dynamo-driven poloidal current is removed. Typical discharges are shown in Fig. 2, where the magnetic fluctuation level, toroidal magnetic flux and boundary voltage temporal traces are plotted for both standard (dashed line) and PPCD (solid line) plasmas. The equilibrium in standard RFP plasmas contains a series of discrete dynamo events (as first reported in Ref. 14) manifested by a step-like increase in toroidal flux accompanying bursts of correlated magnetic field and velocity fluctuations in the MST. In PPCD experiments (solid line, $0.009 \text{ s} \leq t \leq 0.017 \text{ s}$ in Fig. 2), several distinct pulses [capacitor discharges, see Fig. 2(c)] are applied to remove toroidal flux from the machine, Fig. 2(b). The periodic bursts of magnetic fluctuations [Fig. 2(a)] are replaced with a smooth period with a rms amplitude of less than 1%.

We show the dynamo has nearly vanished by independent measurements of the current density, electric field, and resistivity (based on electron temperature and ionic charge) profiles. The data below are accumulated by averaging several hundred similar discharges to compile adequate statistics in the Thomson scattering-measured electron temperature profile.

The resistivity in a torus is modified from that originally given by Spitzer by the existence of trapped particles and non-Maxwellian (fast) particles; both of these factors can exist in the RFP. Routine MST diagnostics were used to measure the average profiles in Fig. 3 to determine the resistivity profile based on neoclassical theory in PPCD discharges. These deuterium discharges (fill pressure of about 0.5 mTorr) have plasma current of 400 kA and an outboard-limited, circular last closed flux surface. Shown are profiles of electron density [Fig. 3(a)] measured with an 11 chord FIR interferometer and the electron temperature profile [Fig. 3(b)]. The effective ionic charge (Z_{eff}) profile [Fig. 3(c)] is deduced from measurement of near-infrared bremsstrahlung; this is accessible only in the extended period of low magnetic fluctuation level. In standard plasmas, pollutant emission from neutral particles (primarily sourced from wall recycling) dominates the target radiation. In PPCD plasmas (with a much lower neutral density) the pollutant emission is about the same level as electron-ion bremsstrahlung, and is sepa-

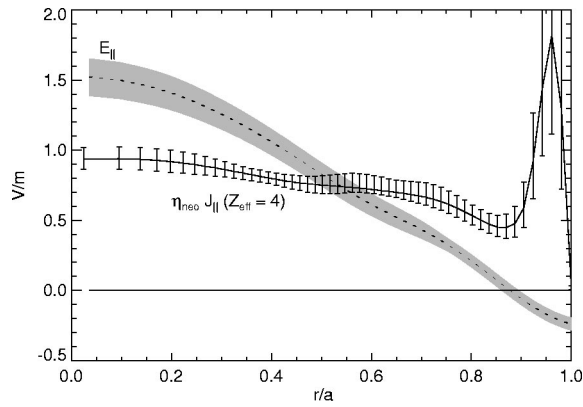


FIG. 1. Imbalance of simple Ohm's law in a standard reversed field pinch. The inductively applied field drives the toroidal plasma current; therefore the parallel (aligned with \mathbf{B}) component of the electric field is negative in the edge due to the reversal of the toroidal magnetic field. This plot contains a measured electric field and current density along with the resistivity profile plotted for an estimated $Z_{\text{eff}}=4$; details can be found in Ref. 15. The parallel component of the electric field changes sign at $r/a \sim 0.9$, where the toroidal component of the magnetic field changes direction. The existence of a layer with zero applied electric field and finite current density illustrates the need for dynamo drive.

rately measured and removed.¹⁵ The trapped particle fraction [Fig. 3(e)] is obtained from two-dimensional equilibrium reconstructions,¹⁶ and the neoclassical resistivity profile¹⁷ is computed including a small correction due to fast particles [Fig. 3(f)]. A measured hard x-ray spectrum and Fokker-Planck modeling indicate up to 20% of the plasma current is carried by fast particles over a small fraction of the minor radius during periods of good confinement;¹⁸ exclusion of this correction does not change our conclusions. The large uncertainty in resistivity at the edge is primarily due to the experimental uncertainty in the edge temperature profile.

The magnetic field and current density profiles are determined via equilibrium reconstruction utilizing the full complement of magnetic and pressure diagnostics on MST.¹⁶ The Grad-Shafranov equation

$$\Delta^* \psi = -\mu_0 R J_\phi, \quad (1)$$

$$J_\phi = \frac{2\pi F F'}{\mu_0 R} + 2\pi R p',$$

specifies the equilibrium (magnetic field and flux, current density, and pressure profiles) when the two free functions ($F = RB_\phi$ and p , pressure) are specified. Here, the elliptic operator $\Delta^* = R^2 \nabla \cdot (\nabla/R^2)$ and ψ is the poloidal magnetic flux; F and p are functions of ψ only and are described by a set of free parameters. The free parameters are varied and on each iteration a comparison to all available data is made. A minimization routine finds the best set of free parameters yielding the best fit equilibrium. Figure 4 contains the magnetic field [Fig. 4(a)] and current density [Fig. 4(b)] profiles required for studying Ohm's law in these PPCD plasmas.

The final element in the Ohm's law analysis is the parallel electric field profile. This is determined in a method similar to that of standard equilibrium reconstruction. The partial derivative of Eq. (1) with respect to time is

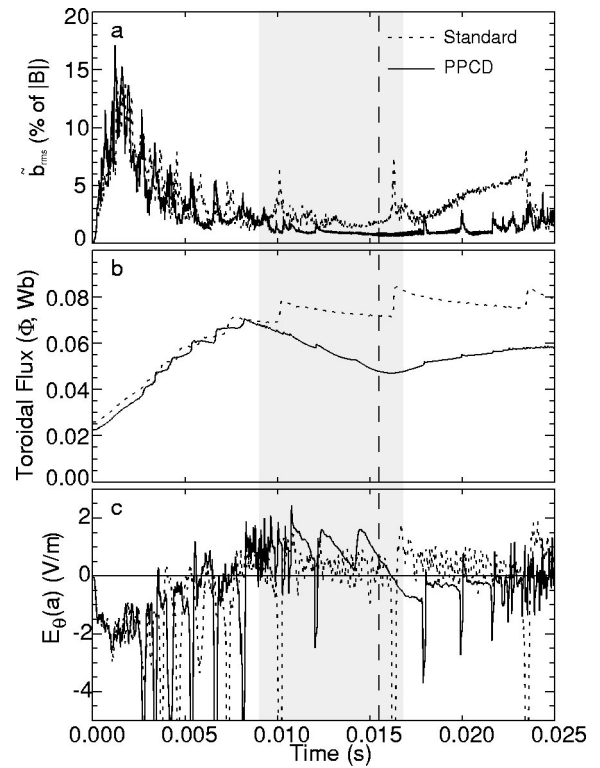


FIG. 2. Operational signals versus time for standard (dotted line) and PPCD (solid line) discharges. Shown are (a) magnetic fluctuation amplitude, (b) toroidal flux, and (c) edge poloidal electric field. Discrete dynamo events, seen as jumps in toroidal flux, coincide with a burst of magnetic fluctuation activity and a large negative spike in poloidal electric field. In PPCD plasmas a positive poloidal electric field is applied from $t = 0.008$ s to $t = 0.017$ s (region shaded in plot), which reduces the toroidal flux and is accompanied by a period of low magnetic fluctuations. The vertical dashed line indicates the time relative to PPCD application when the profiles in Figs. 3–5 are measured.

$$\Delta^* \frac{\partial \psi}{\partial t} = -\mu_0 R \frac{\partial J_\phi}{\partial t}, \quad (2)$$

$$\frac{\partial J_\phi}{\partial t} \Big|_{\mathbf{r}} = \frac{2\pi}{\mu_0 R} \left[\frac{\partial F}{\partial t} \Big|_{\psi} F' + F \frac{\partial F'}{\partial t} \Big|_{\psi} + (F'^2 + FF'') \frac{\partial \psi}{\partial t} \Big|_{\mathbf{r}} \right] + 2\pi R \left(\frac{\partial p'}{\partial t} \Big|_{\psi} + p'' \frac{\partial \psi}{\partial t} \Big|_{\mathbf{r}} \right),$$

where the profiles of F , p' , and ψ (and thus F' , F'' , and p'') are supplied by the equilibrium solution. The two free profiles $\partial F/\partial t$ and $\partial p'/\partial t$ are functions of poloidal flux and are evaluated at a constant poloidal profile. The time derivative of the current density and poloidal flux profiles are computed at fixed spatial points, determined by a grid drawn on the plasma cross section, and hence this method directly incorporates changing flux geometry. Specification of the two free profiles determines the time derivative of the magnetic field and application of Faraday's law immediately yields the toroidal and poloidal electric field profiles. Comparison to the time derivatives of all available magnetic signals on each iteration determines the best fit.

While finite differences of reconstructed equilibria can give meaningful information about Faraday's law for stan-

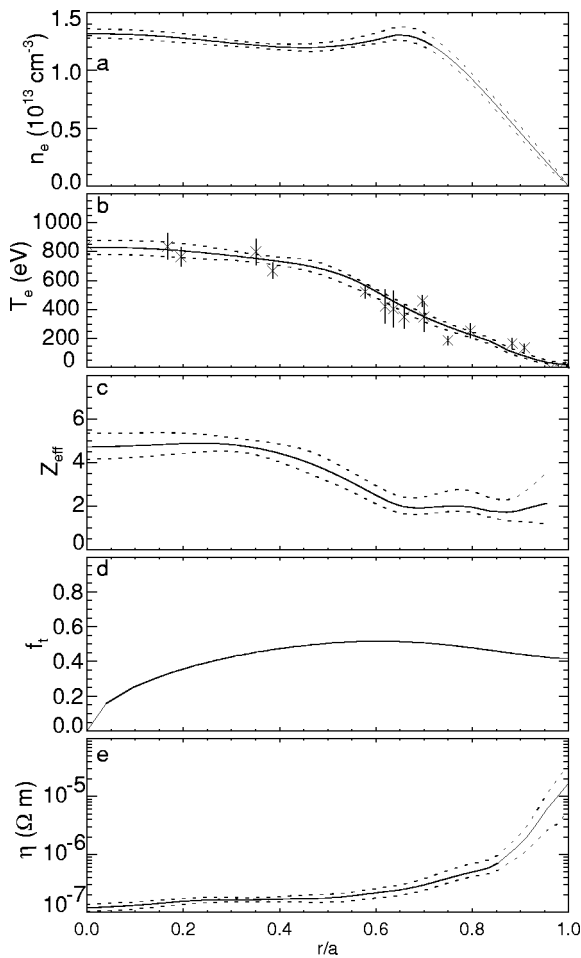


FIG. 3. Profile measurements required to measure the plasma resistivity in PPCD plasmas. These deuterium discharges (fill pressure of about 0.5 mTorr) have plasma current of 400 kA and an outboard-limited, circular last closed flux surface. Shown are (a) electron density, (b) electron temperature, (c) effective ionic charge, (d) trapped particle fraction, and (e) the resistivity profile. Fitting profiles to data with experimental uncertainty leads to the error bars in plots (a) and (b); the error bars in (c) and (e) are the result of propagation of the experimental uncertainty through calculations.

standard plasmas, the above technique is advantageous for PPCD plasmas. In this case, a simple finite difference of reconstructed equilibria fails to give meaningful electric field information as the rapidly changing boundary voltage of PPCD breaks down the assumption of linear flux evolution. Furthermore, this technique is aptly suited to incorporate magnetic data as these are often integrations of induced voltages. Fitting is now performed directly on the measured voltages. Data utilized include the voltages recorded from a poloidal array of Mirnov probes, the time derivative of the total plasma current (voltage from a Rogowski coil), a two-point measurement of the rate of change of on-axis toroidal magnetic field, and boundary voltages.

Figure 4(c) shows the best-fit electric field profiles determined for these PPCD discharges. Plotted are the toroidal (dotted line), poloidal (dashed line), and parallel ($\mathbf{E} \cdot \mathbf{B} / |\mathbf{B}|$, solid line) electric field. The poloidal electric field meets the boundary value of ~ 0.9 V/m and gradually falls to zero at $r/a \sim 0.6$. At this radius (and within), the applied toroidal electric field has a sizable parallel component. Thus the ex-

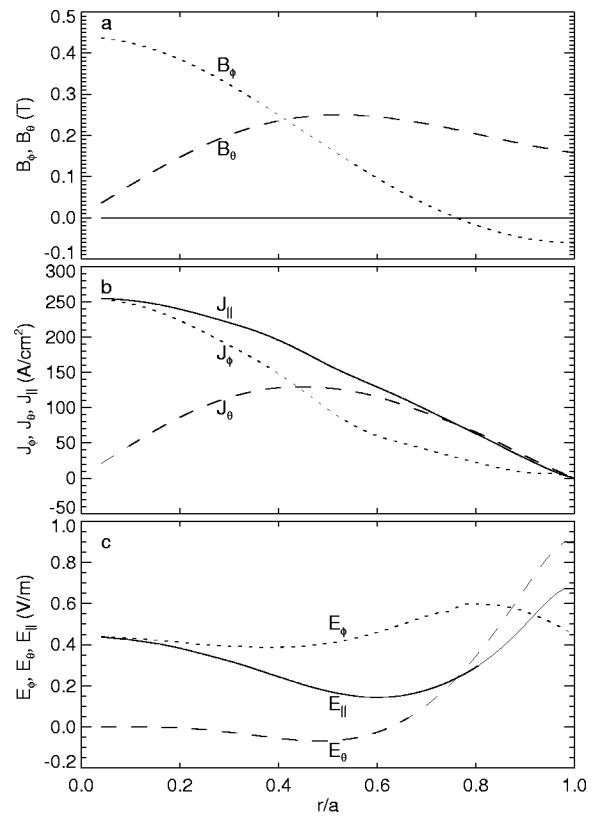


FIG. 4. Equilibrium reconstruction results. Shown are (a) toroidal and poloidal magnetic field profiles; (b) toroidal, poloidal, and parallel ($\mathbf{J} \cdot \mathbf{B} / |\mathbf{B}|$) current density; and (c) toroidal, poloidal, and parallel electric field. In all plots, dotted lines are used for the toroidal component, dashed for poloidal, and solid for parallel.

ternally applied electric field is finite over the entire cross section. This contrasts the standard plasma (shown in Fig. 1), where the applied electric field is zero at the reversal surface and antiparallel in the extreme edge.

The applied parallel electric field nearly matches the product of plasma resistivity and parallel current density over the entire minor radius, or $E_{\parallel} = \eta J_{\parallel}$ as shown in Fig. 5. Thus, the current is essentially accounted for by the applied electric field and the dynamo effect is small. This is in stark

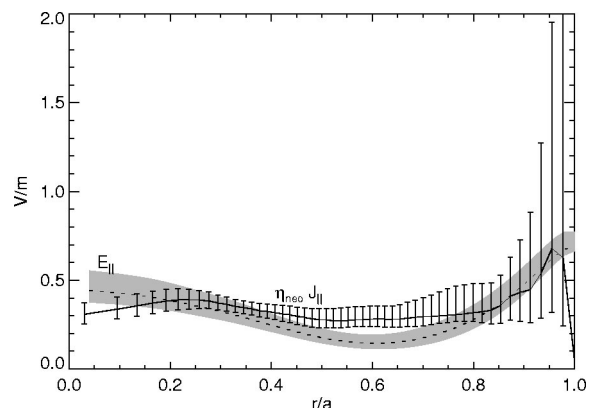


FIG. 5. Balance of simple Ohm's law in PPCD plasma. The inductively applied parallel electric field matches the product of resistivity and current density over the minor radius. In particular, the two quantities agree at the reversal surface ($r/a \sim 0.75$) which cannot occur in standard RFP plasmas.

contrast to the standard RFP (Fig. 1) where the mismatch between E_{\parallel} and ηJ_{\parallel} is large. We also note that the reasonable agreement between the neoclassical resistivity profile based on kinetic measurements and the ratio of the electric field to current density $\eta_{\text{neo}} \approx E_{\parallel} / J_{\parallel}$ implies the neoclassical theory¹⁷ is adequate to describe current diffusion in the RFP.

In summary, this work shows the RFP configuration can transiently exist with nearly zero dynamo-driven current. It remains to be verified that this state can be maintained with some form of steady-state current profile control. The nearly dynamo free plasmas are characterized by low magnetic fluctuation levels, whereas standard plasmas have larger magnetic fluctuation levels and a strong dynamo effect. This is beneficial because RFP confinement is limited by magnetic fluctuations associated with the dynamo current drive. The neoclassical model accurately predicts the resistivity of the reversed field pinch plasma, and in the absence of magnetic fluctuations a simple Ohm's law ($E_{\parallel} = \eta J_{\parallel}$) is satisfied in the Madison Symmetric Torus.

ACKNOWLEDGMENTS

The authors are grateful for the contributions of the UW-Madison MST group and collaborators.

This work was supported by the U.S. Department of Energy, the Oak Ridge Institute for Science and Education Magnetic Fusion Science program, and the National Science

Foundation through the Center for Magnetic Self-Organization.

- ¹J. A. Phillips, D. A. Baker, R. F. Gribble, and C. Munson, *Nucl. Fusion* **28**, 1241 (1988).
- ²J. B. Taylor, *Phys. Rev. Lett.* **33**, 1139 (1974).
- ³H. A. B. Bodin and A. A. Newton, *Nucl. Fusion* **20**, 1255 (1980).
- ⁴K. F. Schoenberg, R. W. Moses, and R. L. Hagenson, *Phys. Fluids* **27**, 1671 (1984).
- ⁵E. J. Caramana and D. A. Baker, *Nucl. Fusion* **24**, 423 (1984).
- ⁶S. C. Prager, *Plasma Phys. Controlled Fusion* **41**, A129 (1999).
- ⁷H. Ji, A. F. Almagri, S. C. Prager, and J. S. Sarff, *Phys. Rev. Lett.* **73**, 668 (1994).
- ⁸C. R. Sovinec and S. C. Prager, *Nucl. Fusion* **39**, 777 (1999).
- ⁹J. S. Sarff, S. A. Hokin, H. Ji, S. C. Prager, and C. R. Sovinec, *Phys. Rev. Lett.* **72**, 3670 (1994).
- ¹⁰R. Bartiromo, V. Antoni, T. Bolzonella *et al.*, *Phys. Plasmas* **6**, 1830 (1999).
- ¹¹M. R. Stoneking, N. E. Lanier, S. C. Prager, J. S. Sarff, and D. Sinitsyn, *Phys. Plasmas* **4**, 1632 (1997).
- ¹²B. E. Chapman, T. M. Biewer, P. K. Chattopadhyay *et al.*, *Phys. Plasmas* **7**, 3491 (2000).
- ¹³R. N. Dexter, D. W. Kerst, T. W. Lovell, S. C. Prager, and J. C. Sprott, *Fusion Technol.* **19**, 131 (1991).
- ¹⁴R. G. Watt and R. A. Nebel, *Phys. Fluids* **26**, 1168 (1983).
- ¹⁵J. K. Anderson, P. L. Andrew, B. E. Chapman, D. Craig, and D. J. Den Hartog, *Rev. Sci. Instrum.* **74**, 2107 (2003).
- ¹⁶J. K. Anderson, C. B. Forest, T. M. Biewer, J. S. Sarff, and J. C. Wright, *Nucl. Fusion* **44**, 162 (2004).
- ¹⁷S. P. Hirshman and D. J. Sigmar, *Nucl. Fusion* **21**, 1079 (1981).
- ¹⁸R. O'Connell, D. J. Den Hartog, C. B. Forest *et al.*, *Phys. Rev. Lett.* **91**, 045002 (2003).